

Improvement in MRS parameter estimation by joint and laterally constrained inversion of MRS and TEM data

Ahmad A. Behroozmand¹, Esben Auken¹, Gianluca Fiandaca^{1,2}, and Anders Vest Christiansen³

ABSTRACT

We developed a new scheme for joint and laterally constrained inversion (LCI) of magnetic resonance sounding (MRS) data and transient electromagnetic (TEM) data, which greatly improves the estimation of the MRS model parameters. During the last few decades, electrical and electromagnetic methods have been widely used for groundwater investigation, but they suffer from some inherent limitations; for example, equivalent layer sequences. Furthermore, the water content information is only empirically correlated to resistivity of the formation. MRS is a noninvasive geophysical technique that directly quantifies the water content distribution from surface measurements. The resistivity information of the subsurface is obtained from a complementary geophysical method such as TEM or DC resistivity methods. The conventional inversion of MRS data assumes the resulting resistivity structure to be

correct and considers a constant MRS kernel through the inversion. We found that this assumption may introduce an error to the forward modeling and consequently could result in erroneous parameter estimations in the inversion process. We investigated the advantage of TEM for the joint inversion compared to DC resistivity. A fast and numerically efficient MRS forward routine made it possible to invert the MRS and TEM data sets simultaneously along profiles. Furthermore, by application of lateral constraints on the model parameters, lateral smooth 2D model sections could be obtained. The simultaneous inversion for resistivity and MRS parameters led to a more reliable and robust estimation of all parameters, and the MRS data diminished the range of equivalent resistivity models. We examined the approach through synthetic data and a field example in Denmark where good agreement with borehole data was demonstrated with clear correlation between the relaxation time T_2^* and the grain size distribution of a sandy aquifer.

INTRODUCTION

Among geophysical methods, the application of electrical and electromagnetic (EM) techniques for near-surface investigations has improved rapidly in the last few decades, because they distinguish between formations of different electrical resistivity. With these methods, electrical resistivity is the key parameter in aquifer characterization. The fact that clayey layers have a lower resistivity than sandy layers enables a distinction between permeable and non-permeable formations. However, water content can only be obtained indirectly from resistivity based on empirical relationships like Archie's law, often resulting in ambiguous interpretations where resistivity contrasts are small (Sørensen et al., 2005; Auken et al., 2006).

Magnetic resonance sounding (MRS) is a relatively new geophysical technique (compared to electrical and EM methods) for groundwater investigation. MRS is unique among EM geophysical methods because it offers a direct quantification of water content from surface measurements. Based on the physical principle of NMR, the transmitter current at a specific frequency generates an energizing magnetic field that excites protons of the water molecules in the subsurface. When the current is switched off, the protons will continue to precess while reverting back to their lower level of energy. This motion generates a secondary magnetic field that induces the voltage response in a receiver loop on the surface (Legchenko and Valla, 2002; Hertrich, 2008).

Manuscript received by the Editor 11 October 2011; revised manuscript received 16 February 2012; published online 9 July 2012.

¹Department of Geoscience, Aarhus University, Denmark. E-mail: ahmad@geo.au.dk; esben.auken@geo.au.dk.

²Department of Mathematics and Informatics, University of Palermo, Italy. E-mail: gianluca.fiandaca@geo.au.dk.

³Geological survey of Denmark and Greenland, Department of Groundwater and Quaternary Geology Mapping, Copenhagen, Denmark. E-mail: avc@geus.dk.

© 2012 Society of Exploration Geophysicists. All rights reserved.

A complementary method like the transient electromagnetic (TEM) or geoelectric (DC resistivity) method is essential for interpretation of the MRS data because the conductivity of the formation determines the excitation magnetic field values in the subsurface and thereby the MRS kernel calculation. In cases where the inversion of TEM/DC resistivity data does not represent the true conductivity structure accurately because of equivalence, the MRS response will be changed due to the wrong estimation of the excitation fields. This effect will be demonstrated using a synthetic example. Similarly, the presence of a deep conductive layer will influence the magnetic field considerably. We will show that this effect may introduce considerable errors in the MRS forward response.

In the conventional stepwise inversion of MRS data (Legchenko and Shushakov, 1998; Mohnke and Yaramanci, 2002; Mohnke and Yaramanci, 2005; Hertrich, 2008; Mueller-Petke and Yaramanci, 2010), the resistivity structure is obtained by inverting, e.g., TEM/DC resistivity data; assuming the model is correct, the MRS kernel is constant through the inversion. Consequently, the MRS inverse problem may lead to erroneous model parameters because an incorrect resistivity structure leads to forward modeling errors.

In this study we present an inversion scheme for joint and laterally constrained inversion (LCI) of MRS and TEM data in which the resistivity structure is inverted simultaneously with the MRS parameters. The resistivity values are updated for each calculation of the MRS forward response in the iterative inversion procedure leading to a more reliable and robust determination of aquifer characteristics. We prefer joint inversion with TEM rather than with DC resistivity because of the greater depth penetration of the former, which is particularly important in the case of a deep good conductor. The 1D-LCI approach (Auken et al., 2005) allows the reconstruction of model sections along profiles of aligned soundings using 1D computations for the forward response and the derivatives of the Jacobian. For the cases where 1D is a valid approximation, as it often occurs in sedimentary environments, the information from areas with well-resolved parameters migrate through the lateral constraints to help resolve the poorly determined parameters, and quasi 2D model sections can be retrieved (Auken et al., 2005; Christiansen et al., 2007).

The inversion scheme uses a new MRS forward routine where data are the full free induction decays (FID), and a stretched-exponential model is used for approximation of multiexponential behavior of the MRS signal (Behroozmand et al., 2011). The MRS forward response is calculated in a numerical efficient manner, which speeds up the computation time considerably and reduces the data and the model space maintaining the numerical accuracy. The fast forward routine makes it feasible to invert MRS and TEM data sets simultaneously along a profile with lateral constraints on the model parameters.

We begin the following sections with a brief introduction to the theory of MRS and TEM forward responses. We describe the inversion algorithm, discuss the need for joint inversion of the MRS data with other geophysical methods, and highlight why we prefer TEM as a complementary method. Subsequently, we present a synthetic example in which results of joint (no LCI) and joint-LCI approaches are compared with those of the stepwise approach, and the improvement in the model parameters is discussed. Finally, we present a field example from Denmark demonstrating the improved resolution obtained with the joint and laterally constrained

approach. Throughout this paper, for the simulation of the MRS response, the pulse moments, time gate values, loop side lengths, etc., are taken from real MRS field surveys.

THE TWO FORWARD PROBLEMS

TEM forward response

The TEM method has been widely used for hydrogeological investigations, both as ground-based and airborne measurements. The method determines the resistivity of the subsurface layers from the surface down to several hundred meters. The injected current in the transmitter loop produces a static primary magnetic field. When the current in the transmitter loop is abruptly shut off, the related change in the primary magnetic field induces an electromotive force in the ground, which results in eddy currents followed by the secondary magnetic field. As time passes, the decaying secondary field induces an electromotive force in the receiver coil. The signal is measured as values of the vertical component of the magnetic field, or of its time derivative as a function of time, and contains the resistivity information of the subsurface. For the central loop configuration used in this study, the data are measured at the center of a rectangular transmitter loop. The later the signal is the measured, the deeper the information obtained (Sørensen and Auken, 2004; Christiansen et al., 2006). The general derivation of the TEM forward response is beyond the scope of this paper. In short, we follow Ward and Hohmann (1988) using Hankel filters (Christensen, 1990) to transform from space domain to frequency domain. Low pass filters are applied in the frequency domain following Effersø et al. (1999) and the frequency to time domain transform is implemented using cosine-sine ($J_{-1/2}, J_{+1/2}$) filters (Johansen and Sørensen, 1979). The transmitter waveform is implemented following Fitterman and Stewart (1986).

MRS forward response

The spin of hydrogen protons of water molecules in the subsurface is the physical property used in MRS applications. Based on the nuclear magnetic resonance (NMR) principle, protons of water molecules in the subsurface are excited at the specific Larmor frequency, which is determined by $|f_L| = \gamma B_0 / 2\pi$. The gyromagnetic ratio for the proton is γ , and B_0 denotes the static magnetic field; here, the local earth's magnetic field. An alternating current tuned at the Larmor frequency is passed through a large transmitter loop laid out on the surface, which generates the excitation magnetic field in the subsurface. This field forces the proton's magnetization vectors away from their initial state along the earth's static magnetic field. After the current is switched off, the protons will continue to precess while gradually reverting back to their equilibrium state along the earth's magnetic field. Finally, the induced voltage response is measured as a superposition of the signals arising from all the precessing nuclear spins within the excited earth volume (Weichman et al., 2000). The initial amplitude of the MRS decaying signal is proportional to the water content, whereas its relaxation time is related to the pore structure of the geological layers (Schirov et al., 1991; Legchenko and Valla, 2002). Although the NMR signal is very small in MRS applications due to the earth's relatively weak magnetic field, a large investigation volume of water in the subsurface makes it possible to measure NMR signals using a loop on the surface. A series of increasing pulse moments, the product of current

amplitude and pulse duration $q = I_0 \cdot \tau$, are passed through the loop to provide depth information.

The entire MRS data set is used in the forward modeling and inversion. The need to do so is highlighted by [Mueller-Petke and Yaramanci \(2010\)](#). Moreover, the measured FIDs are multiexponential in character. The relaxation distribution is often simplified by a Debye relaxation function or described by a multiexponential fit to the data, i.e., assuming a set of relaxation time values (typically equally spaced on a logarithmic time scale) and fit for the amplitudes only. The latter needs a large number of amplitudes to be resolved during the inverse problem. We approximate this complexity of relaxation distribution of the MRS signal in porous media by a stretched-exponential (SE) function ([Kenyon et al., 1988](#)) so that the 1D forward expression is given by ([Behroozmand et al., 2011](#))

$$V(q, t) = \int K(q, z) \cdot W(z) \cdot f(T_2^*(z), C(z)) dz, \quad (1)$$

in which

$$f(T_2^*(z), C(z)) = \exp\left(-\left(\frac{t}{T_2^*(z)}\right)^{C(z)}\right), \quad (2)$$

where $V(q, t)$ is the measured signal depending on pulse moment q and time t . The 1D kernel function and water content distribution are denoted by $K(q, z)$ and $W(z)$, and z is the depth. Equation 2 describes the stretched-exponential model used to approximate the multiexponential behavior of the MRS decays; it is a function of the relaxation time T_2^* and the stretching exponent C which characterizes the deviation of the signal attenuation from monoexponential behavior, and is limited to values between zero and one. A value of C near one indicates high homogeneity, i.e., an almost monoexponential attenuation characteristic of the curve. The underlying assumption in using the SE approach is that the relaxation distribution is monomodal, meaning that one peak exists in the relaxation time distribution. This assumption is acceptable because the measuring time interval of the MRS decays is relatively short, and the first data are typically measured after around 10–40 ms. Under these circumstances, the SE approach provides an acceptable approximation of the complex decay behavior. The model is computationally simple, and the relaxation distribution is approximated by adding a single extra parameter C to the monoexponential modeling.

The forward response is calculated in a numerically efficient manner with respect to the magnetic field computation, discretization, and integration. A piecewise linear transmitter loop is used for calculation of the electromagnetic fields in a stratified earth ([Wannamaker et al., 1984](#); [Xiong, 1989](#)). By taking into account the z -dependence of the upward and downward propagating plane waves of the magnetic-field calculation, the computation time is decreased considerably because the propagating waves are calculated once for each z -plane. Great care is needed in the spatial kernel discretization as the MRS kernel has large variations in the subsurface. Spline interpolation of the MRS kernel helps to effectively reduce the number of discretization points. In addition, a sufficient number of points in each inversion layer is ensured before each forward calculation. These considerations, together with the data and model space reduction and parallelization, allow fast computation while maintaining accuracy. Fast computation becomes important when inverting the MRS data jointly with other geophysical methods in which the MRS kernel has to be computed repeatedly for each resistivity update and for the Jacobian evaluation, and it makes

feasible a joint and laterally constrained inversion of the MRS and TEM data sets.

THE NEED FOR SUFFICIENT DEEP AND CORRECT RESISTIVITY INFORMATION

It has been shown (e.g., by [Braun and Yaramanci, 2008](#)) that information on the resistivity structure is required for the MRS forward calculation because it highly influences the magnetic field values in the subsurface and thereby the MRS kernel calculation. Therefore, complementary data like TEM/DC resistivity are always acquired with the MRS data in the field. The TEM/DC resistivity inversion result, i.e., the estimated resistivity model, is then used in the conventional inversion of the MRS data and assumed to be the correct structure. This means that, in the classic stepwise inversion schemes, the MRS kernel is considered constant during the inversion, and only the hydrological parameters are estimated.

However because of inherent equivalence problems and/or inadequate depth of investigation, the inversion of TEM/DC resistivity does not necessarily deliver the true conductivity structure ([Koefoed, 1979](#); [Sharma and Verma, 2011](#)). As a consequence, an incorrectly estimated resistivity structure may introduce an error in the calculation of the magnetic fields and thereby errors in the MRS forward response. This influences the inversion of MRS data and may result in erroneous model parameters. A detailed example of the influence of the equivalence problem in TEM inversion on the resolution of MRS parameters is presented in the “Synthetic example” section. Here, we show the effect of an insufficient description of the resistivity structure on the MRS kernel. We consider three-layer models containing a deep conductive layer at the bottom, as shown in Figure 1a. Table 1 represents parameter values of models 1–4 in Figure 1a. The resistivity values of the first two layers could represent till and sand saturated with fresh water, whereas the low resistivity of the last layer indicates the same sand layer as in the layer above, but with salt pore water. Model 1 can be considered a result of the inversion of DC resistivity data by which the last layer is not retrieved in the normal field procedure. A water content of 30% is assigned to all layers, and the MRS response is simulated using a 100-m square loop in the earth’s magnetic field of 50,082 nT at an inclination of 70° and a declination of 0°. Four different forward responses are created based on the four models. The differences between the forward response of model 1 and the response of other models are then calculated and shown in Figure 1b–1d by solid circles. They represent the difference in the forward response solely due to the difference in the MRS kernel. We do not show the time axis in the plots because the errors do not vary with time. As the solid circles show, the forward response is considerably changed due to incorrect resistivity information. The relative error decreases as the bottom layer moves deeper. Note that, in models 3 and 4, the deep conductive layer starts below the MRS depth of investigation when it stands alone.

It is noteworthy that these differences will decrease as the resistivity of the last layer increases. To show this, we computed the differences between the forward responses considering resistivity values of 20 and 50 ohm-m in the last layer. The results are shown in Figure 1b–1d by diamonds and asterisks, respectively. Compared to the solid circles, the differences are smaller, but still considerable, particularly for the pulse moments with higher sensitivity to the last layer.

In summary, we argue that the TEM method, due to its superior resolution of deep conductive layers, is the best choice among complementary methods (e.g., DC resistivity) to be used together with MRS to resolve the resistivity structure. Furthermore, we will suggest a method to reduce the equivalence of the resistivity model

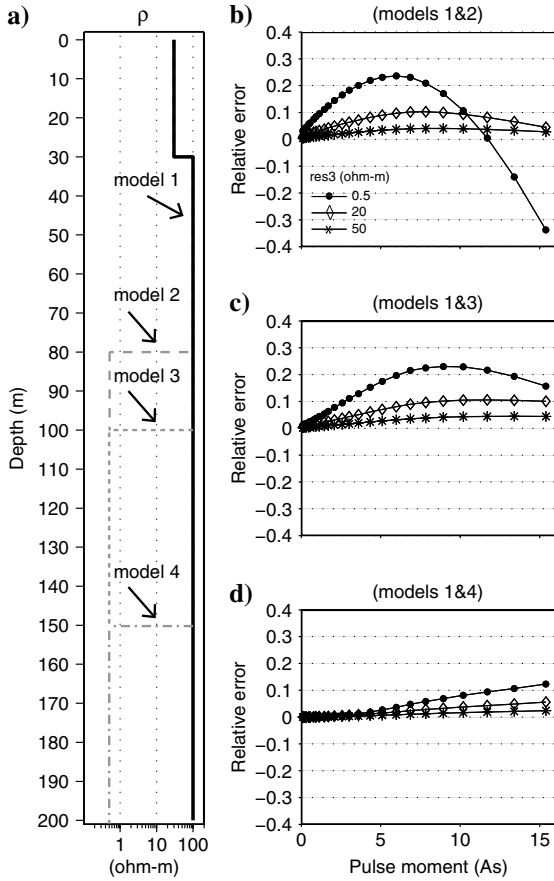


Figure 1. Influence of a deep conductive layer on the MRS kernel. (a) Three-layer models containing a 0.5 Ωm conductive layer at depths of 80, 100, and 150 m, together with a two-layer model 1. Model 1 is considered as a result of, e.g., DC resistivity by which the deep conductive layer is not retrieved. (b, c, d) Solid circles show the difference between the forward response of model 1 and the responses of models 2–4. To show the effect of resistivity, Diamonds and asterisks represent the same differences as the solid circles but considering resistivity values of 20 and 50 ohm-m in the last layer. A 100 m side square loop in the earth's magnetic field of 50,082 nT at an inclination of 70° and a declination of 0° is used for simulation of the response.

Table 1. Parameter values of models 1–4 shown in Figure 1a.

Parameter	Layer 1	Layer 2	Layer 3
ρ (Ωm)	30	100	0.5/20/50
thk -model 1 (m)	30	Inf	—
thk -model 2 (m)	30	50	Inf
thk -model 3 (m)	30	70	Inf
thk -model 4 (m)	30	120	Inf

by performing a joint inversion of the MRS data together with data coming from a complementary method.

INVERSION ALGORITHM

The inversion in this paper has been implemented in the 1D lateral constrained inversion scheme (Auken et al., 2005), retrieving 2D sections in quasilinear environments. In the 1D-LCI algorithm, the model is composed of a set of laterally constrained 1D models aligned along a profile, as sketched in Figure 2.

The MRS data are the entire FIDs integrated over time windows, often called gates (equation 1). For each MRS sounding, a corresponding TEM sounding is used, consisting of apparent resistivity data. The model space consists of a set of models containing the electrical and the MRS parameters, in which the relaxation time distribution is approximated by the stretched-exponential model.

We apply logarithmic data and logarithmic model parameters to impose positivity. Thus, the data space becomes

$$\mathbf{d} = \{(\log(V_{i,j}), \log(\rho_{aK}))_L^T, \quad i = 1, N_q; \quad j = 1, N_{\text{MRS}}; \quad K = 1, N_{\text{TEM}}; \quad L = 1, N_{\text{soundings}}, \quad (3)$$

where N_q , N_{MRS} , N_{TEM} , and $N_{\text{soundings}}$ denote the number of pulse moments, the number of FID gate time values, the number of TEM gate time values (number of TEM data points), and the number of collected 1D soundings. The measured MRS signal dependent on time and pulse moment is represented as $V_{i,j}$, and ρ_a is the apparent resistivity, measured as a function of time. The vector transpose is indicated by T . The common model space contains

$$\mathbf{m} = \{(\log(\rho_i), \log(thk_j), \log(W_i), \log(T_{2i}^*), \log(C_i))_L^T, \quad i = 1, N_{\text{Layers}}, j = 1, N_{\text{Layers}} - 1; \quad L = 1, N_{\text{soundings}}, \quad (4)$$

where ρ , W , T_2^* , C , and thk denote the resistivity, the water content, the relaxation time, the stretching exponent, and the thickness in each layer. A detailed description of the inversion algorithm is presented in Auken and Christiansen (2004) and the following is a brief review. The nonlinear forward mapping of the model to the data space is linearized by the first term of the Taylor expansion. The difference between the observed data and the nonlinear mapping of the model to the data space $\delta\mathbf{d}_{\text{obs}}$ is given by

$$\delta\mathbf{d}_{\text{obs}} = \mathbf{G}\delta\mathbf{m}_{\text{true}} + \mathbf{e}_{\text{obs}}, \quad (5)$$

where $\delta\mathbf{m}_{\text{true}}$ denotes the difference between the true model and an arbitrary reference model, and \mathbf{G} and \mathbf{e}_{obs} represent the Jacobian matrix of the forward mapping and the observation error. Considering a priori information and constraints on the parameters, equation 5 is rewritten in a matrix notation as

$$\begin{bmatrix} \delta\mathbf{d}_{\text{obs}} \\ \delta\mathbf{m}_{\text{prior}} \\ \delta\mathbf{r} \end{bmatrix} = \begin{bmatrix} \mathbf{G} \\ \mathbf{I} \\ \mathbf{R} \end{bmatrix} \cdot \delta\mathbf{m}_{\text{true}} + \begin{bmatrix} \mathbf{e}_{\text{obs}} \\ \mathbf{e}_{\text{prior}} \\ \mathbf{e}_c \end{bmatrix}, \quad (6)$$

in which the first line of the expression relates to the observed data, the second line deals with the a priori information, and the last line considers the constraints. The roughness matrix \mathbf{R} contains the constraints information, and again $\delta\mathbf{m}_{\text{true}}$ represents the difference

between the true model and an arbitrary reference model. The difference between the observed data and the nonlinear mapping of the model to the data space is indicated by $\delta \mathbf{d}_{\text{obs}}$. At the n th iteration we have $\delta \mathbf{m}_{\text{prior}} = \mathbf{m}_n - \mathbf{m}_{\text{prior}}$ and $\delta \mathbf{r}_n = -\mathbf{R} \mathbf{m}_n$; $\mathbf{e}_{\text{prior}}$ and \mathbf{e}_C denote the error on the a priori model and on the constraints with zero as expected value; \mathbf{I} is the identity matrix.

Following the iterative updating inversion scheme, the model update \mathbf{m}_{n+1} is given by

$$\mathbf{m}_{n+1} = \mathbf{m}_n + [\mathbf{G}'^T \mathbf{C}'^{-1} \mathbf{G}'_n + \lambda_n \mathbf{I}]^{-1} \cdot [\mathbf{G}'^T \mathbf{C}'^{-1} \delta \mathbf{d}'_n], \quad (7)$$

where λ denotes the damping factor; the data vector update $\delta \mathbf{d}'_n$ is the collapsed left-hand side of equation 6; \mathbf{G}' is the collapsed \mathbf{G} - \mathbf{I} - \mathbf{R} -matrix in the right-hand side of equation 6; \mathbf{C}' represents the covariance matrix for the joint observation error \mathbf{e}' , which is the last term in equation 6, and is defined in terms of the covariance of the observed data \mathbf{C}_{obs} , the covariance of the a priori information $\mathbf{C}_{\text{prior}}$, and the covariance of the roughness constraints \mathbf{C}_C :

$$\mathbf{C}' = \begin{bmatrix} \mathbf{C}_{\text{obs}} & 0 & 0 \\ 0 & \mathbf{C}_{\text{prior}} & 0 \\ 0 & 0 & \mathbf{C}_C \end{bmatrix}. \quad (8)$$

Equation 7 minimizes the objective function expressed by

$$Q = \left(\frac{1}{N_d + N_m + N_C} [\delta \mathbf{d}'^T \mathbf{C}'^{-1} \delta \mathbf{d}'] \right)^{\frac{1}{2}}, \quad (9)$$

where N_d , N_m , and N_C are the number of data points, the number of a priori constraints on the model parameters and the number of constraints, respectively. Equation 9 without constraints gives the data residual (δ) as

$$\delta = \left(\frac{1}{N_d} [\delta \mathbf{d}_{\text{obs}}^T \mathbf{C}_{\text{obs}}^{-1} \delta \mathbf{d}_{\text{obs}}] \right)^{\frac{1}{2}}. \quad (10)$$

The error on the theoretical description of the forward response, i.e., the structural noise, can be introduced independent of the measured standard deviation through \mathbf{C}_{obs} , as suggested in Tarantola and Valette, (1982b). The resolution of the final inverted model is given by the covariance of the estimation error (Tarantola and Valette, 1982a)

$$\mathbf{C}_{\text{est}} = (\mathbf{G}'^T \mathbf{C}'^{-1} \mathbf{G}')^{-1}, \quad (11)$$

where \mathbf{G}'^T is the first matrix in the right-hand side of equation 6 and \mathbf{C}' is the covariance matrix for the joint observation error.

In the application of joint and 1D laterally constrained inversion (1D-LCI) of MRS and TEM data, all 1D data sets, models, and constraints are considered simultaneously in one inversion procedure, minimizing a common objective function. Each pair of MRS and TEM data sets share a common model, and a lateral smooth transition between the adjacent model parameters is assured as sketched in Figure 2. As a result, a

layered and laterally smooth section provides enhanced resolution of the geological layers because the well-resolved parameters help resolve the poorly determined parameters by migration of information through the lateral constraints.

SYNTHETIC EXAMPLE

To show the improvement of the inversion results by joint inversion of the MRS and TEM data, we simulate a full MRS data set using a square loop with a 100-m loop side over a four-layer model. All measurement parameters have been selected from the field survey presented in the field example, which makes the synthetic data comparable with real field conditions. The earth's magnetic field is set to 50,082 nT at an inclination of 70° and a declination of 0°. The true model, chosen from a real geologic structure in the coastal zone of the Netherlands, is shown in Figures 3, 4a and 5a by dashed gray lines. A 20-m dry sand layer is underlain by a fresh water layer, which is separated from a salt water intrusion by a 3-m clay layer. Table 2 presents the model parameter values. Note that the water content of the second and the third layers does not vary, but the resistivity values are different. In other words, mutual structuring of MRS and resistivity structure do not always occur. In the comparison of the stepwise and joint inversions, the simulated errors play an important role. In particular, in the stepwise approach the noise level of the TEM data controls the quality of the parameter estimation, because highly contaminated data cause significant mis-estimating of the resistivity structure. To avoid this, we decided to use a better situation for the stepwise approach, i.e., noise free data for TEM. In the other case, a Gaussian noise distribution, with a standard deviation of 64 nanovolts (applied to the data before gating) superimposed on a uniform relative noise of 3% of the data values, is added to the MRS forward response. The TEM data set has been simulated for a central loop configuration using a 40-m-square loop as transmitter.

We begin with the conventional stepwise inversion of TEM and MRS data. Using a homogeneous starting model with a resistivity of 50 Ωm for all layers, inversion of the synthetic TEM data results in a

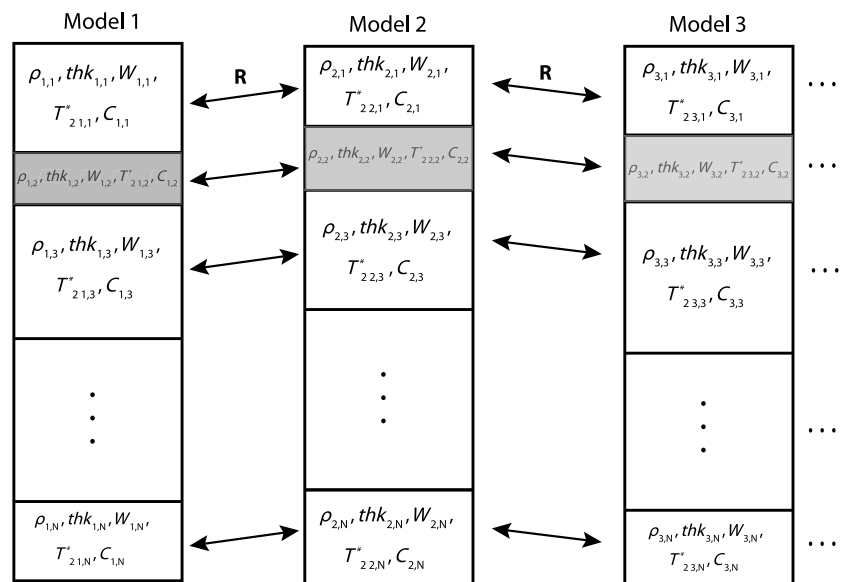


Figure 2. Laterally constrained inversion (LCI) model set-up.

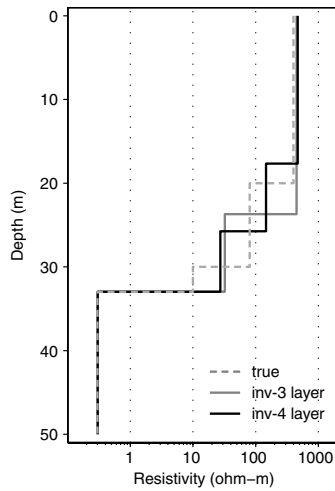


Figure 3. Inversion of TEM synthetic data. Dashed gray line shows the true four-layer model presented in Table 2. Black and solid gray lines denote the four- and three-layer estimated models, respectively. All models simulate closely identical TEM data.

four-layer model, and a data residual of 0.02 is achieved (the data misfit being weighted with 3% of the data values in equation 10). The result is shown in Figure 3, in which the dashed gray line represents the true resistivity model, whereas the black line shows the estimated model. Moreover, to highlight the equivalence problem, a three-layer inversion of the TEM data is shown by the solid gray line. All three models produce nearly identical TEM data. To

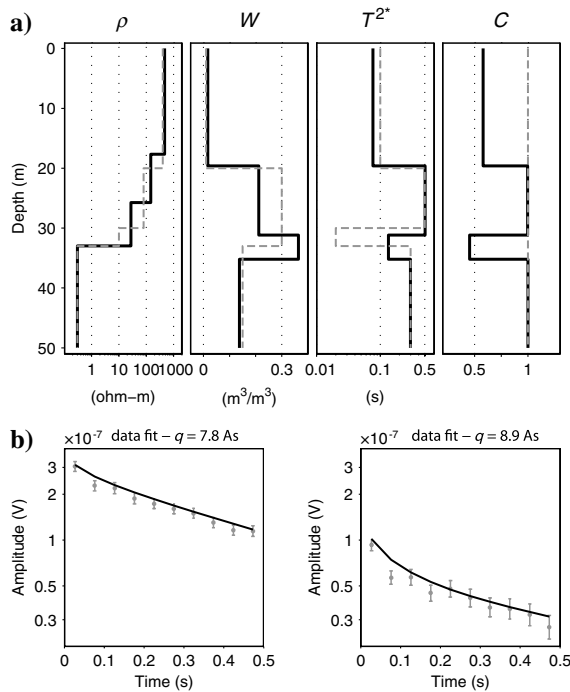


Figure 4. Synthetic example, stepwise inversion of the MRS data. (a) Dashed gray lines show the true model, and black lines represent the inversion results. The model contains four layers with resistivities of 400, 80, 10, and 0.3 Ωm ; water contents of 1, 30, 30, and 15%, relaxation times of 100, 500, 20, and 300 ms; the C parameters of 1 for all layers; and thicknesses of 20, 10, and 3 m, respectively, from top to the bottom. A fixed estimated resistivity structure (from TEM) is considered in the inversion. (b) The fit through two of the FIDs. The TEM data fit is similar to the fit in the joint inversion scheme, as presented in Figure 5c. The response is simulated using a 100-m side-square loop in the earth's magnetic field of 50,082 nT at an inclination of 70°.

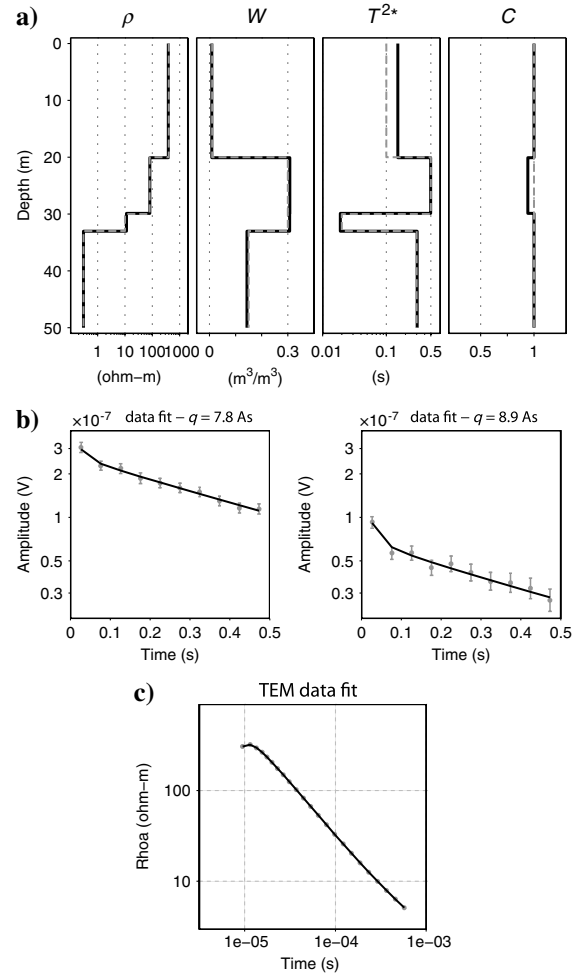


Figure 5. Synthetic example of the joint inversion of the MRS and TEM data. (a) Inversion results; the true model (dashed gray lines, same as Figure 4a) and the inversion results (black lines). (b) The fit through the same FIDs as in Figure 4b. (c) The fit through the TEM data. The field condition is the same as in Figure 4.

Table 2. Model parameter values of the synthetic example

Parameter	Layer 1	Layer 2	Layer 3	Layer 4
ρ (Ωm)	400	80	10	0.3
W (%)	1	30	30	15
T_2^* (ms)	100	500	20	300
C	1.0	1.0	1.0	1.0
thk (m)	20	10	3	Inf

keep the same degree of freedom with the joint inversion, we executed the stepwise inversion considering the estimated four-layer model as a fixed resistivity structure, and inverted solely for the MRS model parameters W , T_2^* , C , and the thicknesses. A homogeneous starting model was used with the starting values of the thicknesses obtained from the inversion of the TEM data. No a priori information nor vertical constraints were applied (as for the TEM inversion). The results are shown in Figure 4a, with black lines showing the inversion results, and dashed gray lines representing the true model. In this case, we get an erroneous estimation; the water content of the first aquifer is underestimated and, more importantly, the clay layer is not retrieved. The water content of the clay is overestimated at 36% and the estimated relaxation time of 135 ms will never indicate clayey context because clay has a T_2^* value below 30 ms (e.g., Schirov et al., 1991). A data residual of 1.52 is obtained. The model response does not fit well through all FIDs, and a bias is observed for some of them. For instance, Figure 4b demonstrates the fit to two of the FIDs. Gray dots denote the data together with their standard deviation, and black lines represent the model response. The vertical axis denotes amplitude of the signal on a logarithmic scale. The TEM data is similarly fitted for both stepwise and joint inversions, as presented in the following figure.

Figure 5 represents the results of joint inversion of the same MRS and TEM data used in Figure 4. A homogeneous starting model was used in which layer boundaries are shared for MRS and TEM models. As Figure 5a shows, the inversion now results in an accurate model estimation. Both aquifers are correctly estimated, and the 3-m clay layer in between is retrieved. Moreover, the data residual is improved by around 50% (0.99). To compare, Figure 5b denotes the fit to the same FIDs as in Figure 4b, which represents a better and nonbiased fit to the data. Figure 5c shows the fit to the TEM data presented as apparent resistivity data (y-axis, logarithmic scale) versus time (x-axis, logarithmic scale). It should be mentioned that in a high-resistive environment the joint approach does not improve the parameter estimations considerably, and the stepwise inversion of the MRS data results in a reasonably accurate estimation of the structure.

Next, we show the improvement in the inversion results by joint and laterally constrained inversion of MRS and TEM data. We selected a four-layer sloped structure expanded from the true model used above. The same parameter values as in Table 2 are assigned to the layers while the thickness of the first layer slightly increases from 14 to 22 m. Note that the structure is simulated by considering five adjacent 1D models, not a full 2D solution. For each 1D model, we simulated the MRS and TEM data, and contaminated them with the same noise structure as above. Figure 6 shows the results as model sections. A vertical exaggeration is applied for better visualization. To investigate the improvement due to the joint and joint-LC inversions, we

compared the results from three different inversions of the data: the conventional stepwise inversion (column 1) in which each MRS data set is inverted independently using fixed resistivity information estimated from TEM models, joint inversion (no LCI) (column 2) in which each MRS/TEM data set is inverted jointly but independent from other data sets, and joint-LCI inversion (column 3) in which all data sets (five MRS and five TEM soundings) are inverted together with application of lateral constraints to the model parameters of each layer. White dashed lines represent the true layer boundaries. A homogeneous starting model is used for all inversions. No a priori information nor vertical constraints were applied. As the left column shows, the stepwise inversion results in erroneous parameter estimations. Section a1 shows the fixed resistivity structure (retrieved from inversion of the TEM data) used during the inversion. Generally, the estimated water content, relaxation time, and C values change considerably within each layer, which is not expected. Moreover, incorrect layer boundaries are estimated through the structure, and the clay layer is not retrieved for models 2, 4, and 5 because they assign a high relaxation time to the layer. Column 2 shows the joint inversion (no LCI) results in which the resistivity and the MRS structures share the same layer

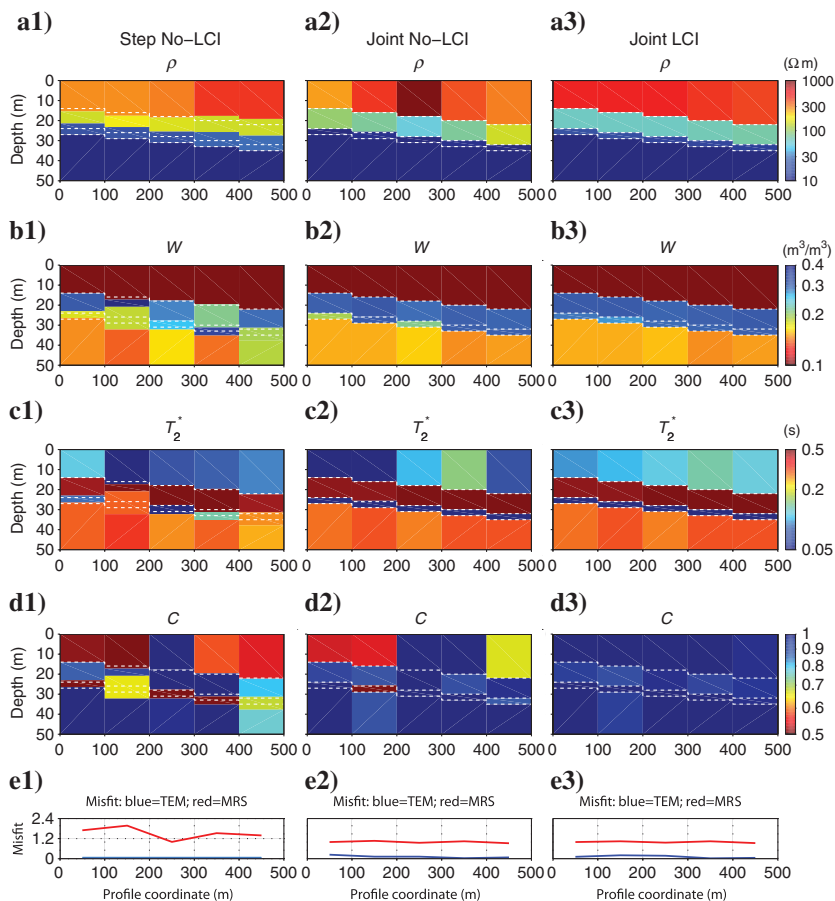


Figure 6. Synthetic example of joint-LCI inversion of the MRS and TEM data. A four-layer sloped structure expanded from the true model used in Figures 4 and 5 is considered as the true structure. The same parameter values as in Figures 4 and 5 are assigned to the layers, whereas the thickness of the first layer slightly increases from 14 to 22 m. Column 1: the stepwise inversion; column 2: the joint inversion (no LCI); column 3: the joint-LCI inversion results. White dashed lines represent the true layer boundaries. Row (e) denotes the data misfit.

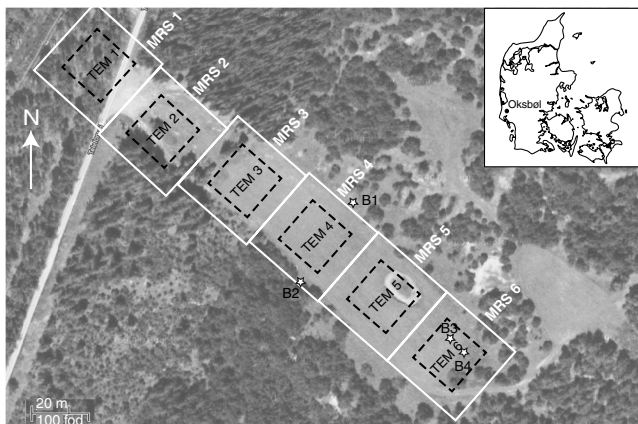


Figure 7. Location map and field set-up of an MRS/TEM survey near Oksbøl, Denmark. White lines and dashed black lines represent the MRS and the TEM loops, respectively, and the asterisks show the location of boreholes along the profile.

boundaries. A considerable improvement in parameter estimations is achieved and the layer boundaries are estimated correctly. However, some features of changes in parameter values within each layer are still apparent. Column 3 represents the results of the joint-LCI approach in which parameters of the adjacent layers are tied together with a lateral constraint of a factor of 1.3 (roughly allowing 30% lateral variations between the constrained parameters). All parameter values and layer boundaries are correctly retrieved and closely identical values are achieved within each layer.

For all the inversions, the TEM model responses fit the data very well, but lower MRS data misfits are obtained in columns 2 and 3.

In summary, the resistivity structure influences the exciting magnetic fields and thereby the MRS kernel. The improvement in the MRS parameter estimations indicates that the MRS data contain information on resistivity and layer boundaries. Therefore, a way to reduce the equivalence of the resistivity model is to perform a joint inversion of the MRS data together with data coming from a complementary method. Moreover, the synthetic joint-LCI example shows that the lateral constraints further improves the parameter estimation by contributing information on the lateral coherency of

the expected model. The lateral constraints thereby ensures migration of information which helps resolve the poorly determined parameters.

FIELD EXAMPLE

For the field example, we will show the results from a MRS/TEM survey near Oksbøl in Denmark. For the purpose of evaluating the joint and laterally constrained scheme, the survey was conducted along a 300 m profile, containing six edge-to-edge MRS soundings and six corresponding TEM soundings. The MRS measurements were performed using the NUMIS Poly system (IRIS Instruments; sampling rate of 19,200 Hz) and the conventional coincident Tx/Rx loop configuration. For TEM measurements, we used the WalkTEM instrument, developed at the Department of Geoscience, Aarhus University. It employs a 40 by 40-m-square transmitter loop. It measures using a low and a high moment of 1A and 8A (magnetic moments of 1600 and 12,800 Am²). The transmitted current waveform is an alternating square wave with 10-ms current on time followed by 10-ms measuring time. A central loop configuration was used for measurements, in which a receiver coil with effective area of 5 m² is located in the center for measuring the transient earth response (Nyboe et al., 2010). The location map of the area is depicted in Figure 7. White lines show the MRS 50-m-side square loops, and dashed black lines show the TEM 40-m-side transmitter loop. The location of four boreholes along the profile is shown by asterisks. The boreholes were drilled by cable percussion method and have accuracy in the range of a few centimeters (A. G. Cahill, personal communication, 2012).

Prior to the inversion, the measured MRS data were processed. The processing consists

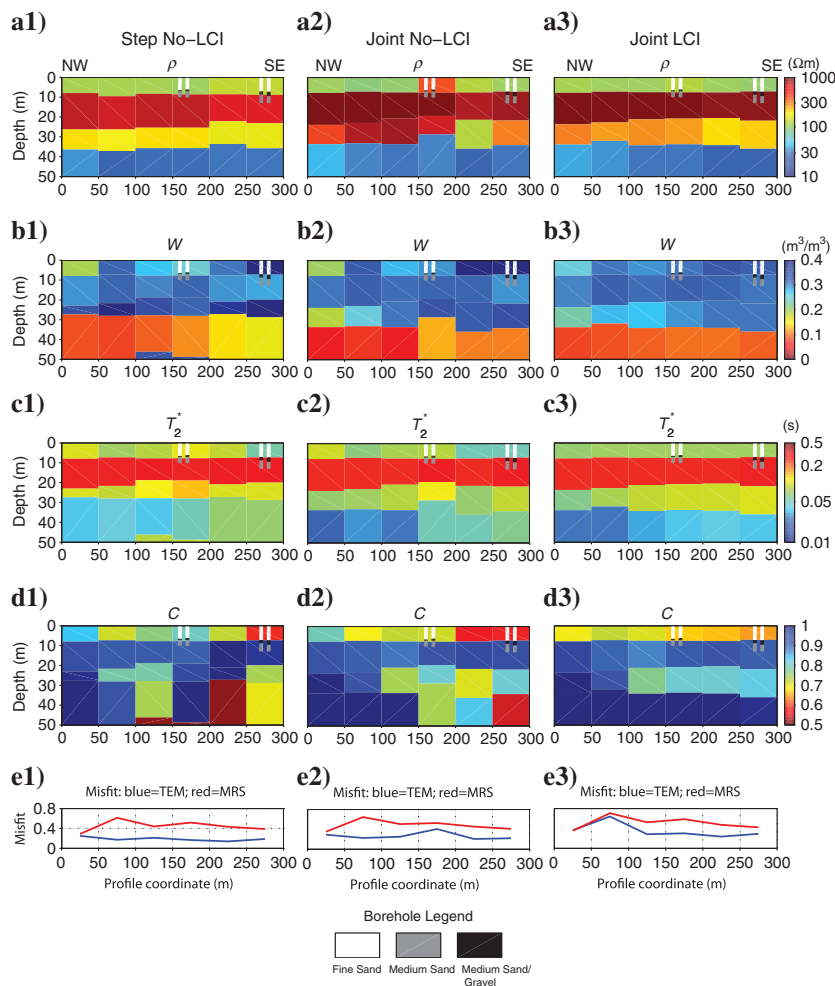


Figure 8. Inversion results of the MRS/TEM field data. Column 1: the stepwise approach; column 2: the joint approach (no LCI); column 3: the joint-LCI approach. The boreholes data are plotted on top of the sections, and the legend is shown at the bottom of the figure.

of despiking, Wiener filtering to detect and eliminate the power line contamination, and a stacking procedure to eliminate stochastic noise. After this three-step processing, the signal amplitudes are detected by the digital quadrature detection (Levitt, 1997) and integrated over 10 time windows. Processing of the MRS data is beyond the scope of this paper and is properly described in, e.g., Walsh (2008), Dlugosch et al. (2011) and Mueller-Petke et al. (2011).

Similar to the synthetic example, we compared the results of stepwise, joint (no LCI), and joint-LCI approaches, shown in Figure 8 as model sections, together with the information from the four boreholes along the profile. Before the few-layer inversion of the data and to obtain a general overview of the structure, we first inverted each of the MRS/TEM data sets with a smooth model, in which vertical constraints for model parameters (vertical smoothing) are used, and the model depth discretization does not change during the inversion. Based on that, the model parameters and the layer boundaries for the starting models were obtained.

For stepwise inversion (column 1) of each MRS data set, a good misfit is obtained for both MRS and TEM data (Figure 8e1). The resistivity models (Figure 8a1) represent different structure, in terms of layer thicknesses, than MRS models (Figure 8b1–8d1), and the first layer thickness does not agree well the information from the four boreholes along the profile. The joint (no LC) inversion results are shown in column 2. Although a significant improvement is not expected due to the high resistivity values in the top three layers, a better estimation of the first layer thickness is achieved. The boundary to the second layer now agrees well with the borehole information. For the joint-LCI approach, all the 1D data sets and models have been inverted in one attempt. No a priori constraints are applied to the model parameters, and parameters of the adjacent layers are tied together with a lateral constraint of a factor of 1.3. The results are shown in column 3 in Figure 8. The mean value of the model parameters in each layer is shown in Table 3. The first layer has medium resistivity, contains 30% water and is 7.5 m thick. The second layer is resistive and is similar to the first layer in terms of the water content. In contrast, a much higher value is achieved for the relaxation time, which indicates the larger pore structure in the second layer compared to the first layer. This is in very good agreement with the information from the four boreholes along the profile. The first layer consists of fine sands, whereas the second layer contains medium sand and some gravel. Moreover, a higher value of the C parameter represents a more homogeneous layer compared to the first one. The third layer is more conductive and shows a decrease in the water content, relaxation time, and the C values. Finally, the fourth layer is conductive, has low water content and relaxation time values, and is considered to be a clay layer. A total residual of 0.48 is achieved. The inversion results of the third and the fourth MRS soundings in column 1 estimate the boundary to the bottom layer below 50-m depth. This layer is considered in the inverse problem because it is needed for inversion of the TEM data sets, to provide deep resistivity information.

Figure 9a shows the fit to all MRS data sets in the joint-LCI approach. Black dots denote the observed data and gray lines represent the model response. As the figure shows, all the FIDs are fitted well and good data residuals are obtained. Similarly, the fits through all TEM data sets are depicted in Figure 9b, also with a good data residual. Black and gray colors denote the low and the high moment data, respectively.

Table 3. Mean values of the model parameters of the field example

Parameter	Layer 1	Layer 2	Layer 3	Layer 4
ρ (Ωm)	110	987	265	31
W (%)	30	31	27	8
T_2^* (ms)	73	274	85	33
C	0.7	0.9	0.86	1
thk (m)	7.5	14.3	12.1	Inf

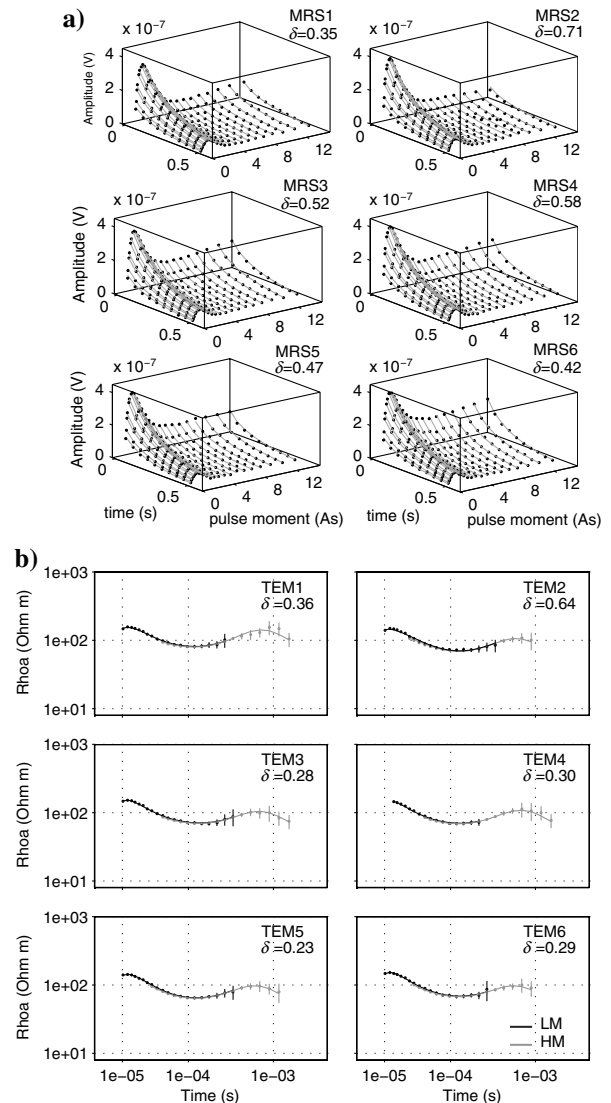


Figure 9. The fit through (a) the individual MRS and (b) TEM field data, together with their residuals (δ). (a) Black dots denote the observed data and gray lines represent the model response. (b) Black and gray colors show the low and high moment data and the corresponding model responses. All data are fitted in one inversion procedure.

CONCLUSION

A joint and laterally constrained inversion of MRS and TEM data is presented and the improvement in the inversion results is demonstrated. We highlight the resistivity information of the MRS data, which helps the model to be updated correctly during the joint inversion. As a result, a more reliable determination of aquifer characteristics is achieved compared to the stepwise inversion of the MRS data, and the equivalence of the resistivity model is diminished. We have discussed the need for sufficient deep and correct resistivity information, and in light of that, we argue the advantage of TEM compared to DC resistivity in a joint inverse problem. The results are improved considerably when highly conductive layers exist. The improvement in parameter estimation is investigated by a synthetic example in which the results from the stepwise, joint (no LCI), and joint-LCI approaches show a better estimation of the parameter values and the layer thicknesses when we jointly invert the MRS and TEM data. Moreover, with application of LC on the parameters of the adjacent layers, the joint-LCI approach results in a reasonably accurate estimation of the structure in which closely identical values are achieved within each layer. The field example results are shown to compare favorably with in-site boreholes for the joint-LCI approach, although the resistivity effect is less pronounced due to generally high resistivities.

ACKNOWLEDGMENTS

This work was carried out as part of the RiskPoint project (assessing the risks posed by point source contamination to groundwater and surface water resources), supported by the Danish Agency for Science Technology and Innovation under grant number 09-063216, and the CO₂-GS project, supported by a grant of the Danish Council of Strategic Research (DSF-09-067234). We would like to thank Niels B. Christensen, Aarhus University, for thorough review of the manuscript. We thank James Ramm and Jesper Pedersen, Aarhus University, for their help in the field, Esben B. Dalgaard, Aarhus University, for processing the data, and Aaron Cahill, Technical University of Denmark, for providing borehole information. The authors thank the editors and reviewers for their fruitful comments and thorough review of the manuscripts.

REFERENCES

- Auken, E., K. I. Sørensen, and A. V. Christiansen, 2006, Structural mapping of large aquifer structures, 19th Annual Symposium on the Application of Geophysics to Engineering and Environmental Problems (SAGEEP), SS-03.
- Auken, E., and A. V. Christiansen, 2004, Layered and laterally constrained 2D inversion of resistivity data: *Geophysics*, **69**, 752–761, doi: [10.1190/1.1759461](https://doi.org/10.1190/1.1759461).
- Auken, E., A. V. Christiansen, B. H. Jacobsen, N. Foged, and K. I. Sørensen, 2005, Piecewise 1D laterally constrained inversion of resistivity data: *Geophysical Prospecting*, **53**, 497–506, doi: [10.1111/gpr.2005.53.issue-4](https://doi.org/10.1111/gpr.2005.53.issue-4).
- Behroozmand, A. A., E. Auken, G. Fiandaca, E. Dalgaard, and J. Larsen, 2011, Full free induction decay (FID) inversion of MRS data, 17th European Meeting of Environmental and Engineering Geophysics.
- Braun, M., and U. Yaramanci, 2008, Inversion of resistivity in magnetic resonance sounding: *Journal of Applied Geophysics*, **66**, 151–164, doi: [10.1016/j.jappgeo.2007.12.004](https://doi.org/10.1016/j.jappgeo.2007.12.004).
- Christensen, N. B., 1990, Optimized fast Hankel transform filters: *Geophysical Prospecting*, **38**, 545–568, doi: [10.1111/gpr.1990.38.issue-5](https://doi.org/10.1111/gpr.1990.38.issue-5).
- Christiansen, A. V., E. Auken, N. Foged, and K. I. Sørensen, 2007, Mutually and laterally constrained inversion of CVES and TEM data — A case study: *Near Surface Geophysics*, **5**, 115–124.
- Christiansen, A. V., E. Auken, and K. I. Sørensen, 2006, The transient electromagnetic method, *in* R. Kirsch, Ed., *Groundwater geophysics*. A tool for hydrogeology: Springer.
- Dlugosch, R., M. Mueller-Petke, T. Günther, S. Costabel, and U. Yaramanci, 2011, Assessment of the potential of a new generation of surface nuclear magnetic resonance instruments: *Near Surface Geophysics*, **9**, 89–102.
- Effersø, F., E. Auken, and K. I. Sørensen, 1999, Inversion of band-limited TEM responses: *Geophysical Prospecting*, **47**, 551–564, doi: [10.1046/j.1365-2478.1999.00135.x](https://doi.org/10.1046/j.1365-2478.1999.00135.x).
- Fitterman, D. V., and M. T. Stewart, 1986, Transient electromagnetic sounding for groundwater: *Geophysics*, **51**, 995–1005, doi: [10.1190/1.1442158](https://doi.org/10.1190/1.1442158).
- Hertrich, M., 2008, Imaging of groundwater with nuclear magnetic resonance: Progress in Nuclear Magnetic Resonance Spectroscopy, **53**, 227–248, doi: [10.1016/j.pnmrs.2008.01.002](https://doi.org/10.1016/j.pnmrs.2008.01.002).
- Johansen, H. K., and K. I. Sørensen, 1979, Fast Hankel transforms: *Geophysical Prospecting*, **27**, 876–901, doi: [10.1111/gpr.1979.27.issue-4](https://doi.org/10.1111/gpr.1979.27.issue-4).
- Kenyon, W. E., P. I. Day, C. Straley, and J. F. Willemsen, 1988, Three-part study of NMR longitudinal relaxation properties of water-saturated sandstones: *SPE Formation Evaluation*, **3**, 622–636, doi: [10.2118/15643-PA](https://doi.org/10.2118/15643-PA).
- Koefoed, O., 1979, *Geosounding principles: 1. Resistivity sounding measurements*: Elsevier.
- Legchenko, A., and P. Valla, 2002, A review of the basic principles for proton magnetic resonance sounding measurements: *Journal of Applied Geophysics*, **50**, 3–19, doi: [10.1016/S0926-9851\(02\)00127-1](https://doi.org/10.1016/S0926-9851(02)00127-1).
- Legchenko, A. V., and O. A. Shushakov, 1998, Inversion of surface NMR data: *Geophysics*, **63**, 75–84, doi: [10.1190/1.1444329](https://doi.org/10.1190/1.1444329).
- Levitt, M. H., 1997, The signs of frequencies and phases in NMR: *Journal of Magnetic Resonance*, **126**, 164–182, doi: [10.1006/jmre.1997.1161](https://doi.org/10.1006/jmre.1997.1161).
- Mohnke, O., and U. Yaramanci, 2002, Smooth and block inversion of surface NMR amplitudes and decay times using simulated annealing: *Journal of Applied Geophysics*, **50**, 163–177, doi: [10.1016/S0926-9851\(02\)00137-4](https://doi.org/10.1016/S0926-9851(02)00137-4).
- Mohnke, O., and U. Yaramanci, 2005, Forward modeling and inversion of MRS relaxation signals using multi-exponential decomposition: *Near Surface Geophysics*, **3**, 165–185.
- Mueller-Petke, M., R. Dlugosch, and U. Yaramanci, 2011, Evaluation of surface nuclear magnetic resonance-estimated subsurface water content: *New Journal of Physics*, **13**, 2802–2804.
- Mueller-Petke, M., and U. Yaramanci, 2010, QT inversion — Comprehensive use of the complete surface NMR data set: *Geophysics*, **75**, WA199–WA209, doi: [10.1190/1.3471523](https://doi.org/10.1190/1.3471523).
- Nyboe, N. S., F. Jørgensen, and K. I. Sørensen, 2010, Integrated inversion of TEM and seismic data facilitated by high penetration depths of a segmented receiver setup: *Near Surface Geophysics*, **8**, 467–473.
- Schirov, M. D., A. Legchenko, and G. Creer, 1991, A new non-invasive groundwater detection technology for Australia: *Exploration Geophysics (USSR)*, **22**, 333–338, doi: [10.1071/EG991333](https://doi.org/10.1071/EG991333).
- Sharma, S. P., and S. K. Verma, 2011, Solutions of the inherent problem of the equivalence in direct current resistivity and electromagnetic methods through global optimization and joint inversion by successive refinement of model space: *Geophysical Prospecting*, **59**, 760–776, doi: [10.1111/gpr.2011.59.issue-4](https://doi.org/10.1111/gpr.2011.59.issue-4).
- Sørensen, K. I., and E. Auken, 2004, SkyTEM — A new high-resolution helicopter transient electromagnetic system: *Exploration Geophysics (USSR)*, **35**, 191–199.
- Sørensen, K. I., E. Auken, N. B. Christensen, and L. Pellerin, 2005, An integrated approach for hydrogeophysical investigations: New technologies and a case history *in* D. K. Butler, ed., *Near-surface geophysics part II: SEG*.
- Tarantola, A., and B. Valette, 1982b, Inverse problems = quest for information: *Journal of Geophysics*, **50**, 159–170.
- Tarantola, A., and B. Valette, 1982a, Generalized nonlinear inverse problems solved using a least squares criterion: *Reviews of Geophysics and Space Physics*, **20**, 219–232, doi: [10.1029/RG020i002p0219](https://doi.org/10.1029/RG020i002p0219).
- Walsh, D. O., 2008, Multi-channel surface NMR instrumentation and software for 1D/2D groundwater investigations: *Journal of Applied Geophysics*, **66**, 140–150, doi: [10.1016/j.jappgeo.2008.03.006](https://doi.org/10.1016/j.jappgeo.2008.03.006).
- Wannamaker, P. E., G. W. Hohmann, and W. A. SanFilipo, 1984, Electromagnetic modeling of three-dimensional bodies in layered earths using integral equations: *Geophysics*, **49**, 60–74, doi: [10.1190/1.1441562](https://doi.org/10.1190/1.1441562).
- Ward, S. H., and G. W. Hohmann, 1988, Electromagnetic theory for geophysical applications, *in* M. N. Nabighian, ed., *Electromagnetic methods in applied geophysics*: SEG.
- Weichman, P. B., E. M. Lavelly, and M. H. Ritzwoller, 2000, Theory of surface nuclear magnetic resonance with applications to geophysical imaging problems: *Physical Review E (Statistical Physics, Plasmas, Fluids, and Related Interdisciplinary Topics)*, **62**, 1290–1312, doi: [10.1103/PhysRevE.62.1290](https://doi.org/10.1103/PhysRevE.62.1290).
- Xiong, Z., 1989, Electromagnetic fields of electric dipoles embedded in a stratified anisotropic earth: *Geophysics*, **54**, 1643–1646, doi: [10.1190/1.1442633](https://doi.org/10.1190/1.1442633).